https://doi.org/10.32441/kjps.06.01.p2

Al-Kitab Journal for Pure Sciences
ISSN: 2617-1260 (print), 2617-8141(online)
www.kjps.isnra.org

Bismuth oxyiodide nanocomposites supported on strontium hydroxyapatite enhance UV-Vis light-driven photocatalytic activity

*Mohammed K. Kzar, Zaki N. Kadhim, Ali H. Al-Mowali

Department of Chemistry,College of Science, University of Basrah, Basrah, Iraq

*Corresponding Author: mohammedkadhikzar@utq.edu.iq

Citation: Kzar M. K., Kadim Z. N., Al-Mowali A. H. Bismuth oxyiodide nanocomposites supported on strontium hydroxyapatite enhance UV-Vis light-driven photocatalytic activity. Al-Kitab Journal for Pure Sciences (2022); 6(1): 14-29. DOI: https://doi.org/10.32441/kjps.06.01.p2.

Keyword
Bismuth Oxyiodide (BiOl), Strontium Hydroxyapatite (SrHA), Cationic Dyes, Photocatalytic, XRD, EDX, and SEM.

Article History

Received	02 May	2022
Accepted	08 July	2022
Available online	02 August	2022

Abstract:

In this research, we discuss the removal of basic fusion (BF), and crystal violet (CV) dyes by strontium hydroxyapatite supported BiOI. In a modified hydrothermal model, one can synthesize BiOI/SrHA. BiOI/SrHA was characterized using Fourier transform-infrared spectroscopy (FTIR), UV-visible (UV-vis) analysis, X-ray diffraction (XRD), energy diffraction X-ray (EDX), and scanning electron microscopy (SEM). SEM outcome confirmed the dispersion of BiOI onto strontium hydroxyapatite. The shape of the BiOI catalytic samples overlapped with each other to form 3D hierarchical flower-like structures. The UV-visible was used as a radiation source during photocatalysis. BiOI/SrHA had an effect on malachite green dye degradation. The oxidative removal occurred through hydroxyl radical formation. UV-visible (UV-vis) BiOI/SrHA showed perfect photocatalytic property for the decay of Basic Fuchsin (BF) and Crystal Violet (CV) from an aqueous solution. According to kinetics analysis, the dye degradation rates could be in a pseudo-first-order model.

Keywords: Bismuth Oxyiodide (BiOl), Strontium Hydroxyapatite (SrHA), Cationic Dyes, Photocatalytic, XRD, EDX, SEM.

مركبات البزموت أوكسي يوديد النانوية المستندة على هيدروكسيباتيت السترونتيوم لتعزز نشاط التحفيز الضوئي بواسطة اشعة *UV-Vis*

محمد كاظم كزار*، زكى ناصر كاظم، على حسين الموالى

قسم الكيمياء، كلية العلوم، جامعة البصرة، البصرة، العراق

*mohammedkadhikzar@utq.edu.iq

Zaki.kadhim@uebasreh.edu.iq / ali-almoaali1946@yaho.com

الخلاصة:

في هذا البحث، نناقش إزالة صبغات الفوكسين الأساسي (BF) والبنفسجي البلوري (CV) بواسطة هيدروكسيباتيت السترونتيوم المستندة على BIOI. بواسطة التحلل الحراري المعدل، يمكن تحضير BIOI / SRHA. تم تشخيص BIOI / SRHA باستخدام التحليل الطيفي بالأشعة تحت الحمراء المحولة من فورييه (FTIR)، وتحليل الأشعة فوق البنفسجية المرئية (UV-VIS)، وحيود الأشعة السينية (XRD)، والأشعة السينية لحيود الطاقة (EDX)، والمجهر الإلكتروني الماسح (SEM). أكدت نتائج SEM تشتت BIOI على هيدروكسيباتيت السترونتيوم. تداخل شكل العينات الحافزة BIOI مع بعضها البعض لتشكيل هياكل D3 الهرمية الشبيهة بالزهور. تم استخدام الأشعة فوق البنفسجية المرئية كمصدر إشعاعي أثناء التحفيز الضوئي. كان ل BIOI / SRHA تأثير على تدهور صبغات الفوكسين الأساسي (BF) والبنفسجي البلوري (CV). حدثت إزالة الأكسدة من خلال تشكيل جذر الهيدروكسيل. أظهرت BIOI / SRHA المرئية للأشعة فوق البنفسجية (UV-VIS) خاصية مثالية للتحفيز الضوئي لاضمحلال الفوكسين الأساسي (BF) والبنفسجي البلوري (CV) من محلول مائي. وفقا لتحليل الحركية، معدل ازالة هذه الاصباغ يمكن تطبيق معادلة درجة الاولى الكاذبة.

الكلمات المفتاحية: أوكسي يوديد البزموت (BiOl)، هيدروكسيباتيت السترونتيوم (SrHA)، الأصباغ الكاتيونية، التحفيز الضوئي، XRD، EDX، SEM.

1. INTRODUCTION:

Pollutants can be elements, molecules, or particles with greatly benefit on living organisms and cause problems for the environment [1]. Plants and trees cannot grow in the absence of clean water. That is, there is no source of food, and this, in turn, can affect the economic conditions of humans, and here we must admit that people are the main source of environmental pollution [2]. One of the most important water pollutants are includes insecticides and herbicides, nutrition processing waste, pollutants from cattle operations, volatile organic compounds, heavy metals, chemical waste, and others [3,4]. Recently, the world has paid a lot of attention to the photocatalytic process. In this field researchers and scientists have conducted many types of experimental research. Heterogeneous photocatalysis is a promising new alternative method for the removal of organic pollutants from water. The photocatalytic mechanism is based on the advanced oxidation process (AOP), which has shown a high ability to decompose, mineralize harmful organic and inorganic compounds in the environment. One of the most important compounds that are used in the photocatalytic process is TiO_2 and ZnO, the importance of these two compounds is their non-toxicity and because of their strong

oxidizing power. The incorporation of bismuth into a given material yields an additional filled Bi 6s state, which appears to be more than O 2p. The transition to the s/d states of a transition metal from Bi 6s (or hybrid Bi 6s–O 2p states) becomes possible, which decreases the band gap. Compounds of the bismuth oxyhalide (BiOX) group exhibit some semiconducting and optical properties. In 1935, the scientist Bannister discovered the BiOX crystal structure and found that it possessed layers linked by covalent bonds of the three elements that made up [X-Bi-O-Bi- X, and X= halogens Cl, Br, I respectively] **[5,6]**. The geometric structure of BiOl/SrHA is tetragonal, so an electric field can be generated by work that activates photocatalytic thus preventing recombination between electrons and Holes formation **[7]**. Zhang et al. (2006) investigated the photocatalytic properties of bismuth oxyiodide (BiOl) as the first BiOX compound **[8]**. In recent years, there have been numerous medical, domestic, and industrial pollution problems. So as a result, efforts have been made to address this serious issue through practical research **[9]**. In this field, nanoparticles have been used extensively to reduce this dangerous phenomenon **[10]**. Many nanomaterials have been used, including bismuth oxyhalide BiOX, the unusual properties of these compounds made them distinguished in this field (passive voice and active voice). The formed Bi nanoparticles in the BiOl surface accelerate the transfer of photo-induced electrons from BiOl to Bi, and the surface oxygen vacancies in the BiOl photocatalyst result in its bandgap narrowing down to the visible light range **[11]**. Many experiments have been conducted in the process of replacing the element strontium (Sr^{+2}) to replace the element calcium (Ca^{+2}) in the compound hydroxyapatite, particularly in biological experiments, specifically in bones, where experiments have proven that the element strontium (Sr^{+2}) is non-toxic and stable when bound to hydroxyapatite **[12-16]**. BiOI displays a small bandgap (~1.7 eV) and is an active visible light photocatalyst for the photodegradation of different pollutants **[17-19]**. Li et.al offers BiOI with 3D hierarchical structures applied in the degradation of methyl orange (MO) and phenol with effective photocatalytic action **[20]**. Zan et.al elucidate that the photodegradation efficiency of cationic Rhodamine B (RhB) with BiOI was remarkably increased highly due to its distinctive structure containing single crystal nanosheets with high symmetry **[21]**. The structure of the two dyes examined is depicted in **Figure1**.

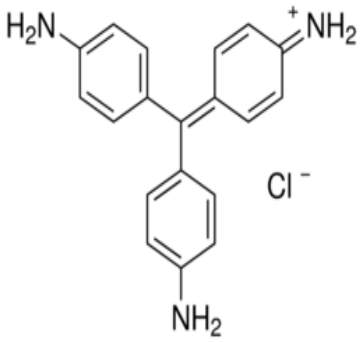

Basic Fuchsin (BF)

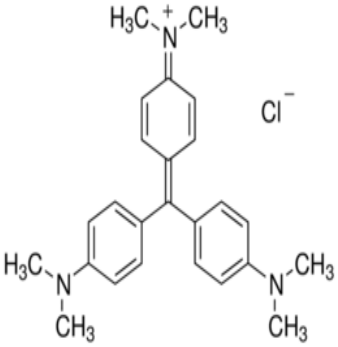

Crystal Violet (CV)

Figure 1: The chemical structure of dyes

2 .Experimental

2.1. Preparation of SrHA

A solution of H_3PO_4 0.3 mol. L-1 was vigorously mixed with a solution of Sr $(NO_3)_2$ 0.5 mol. L-1 (Merck, 99.67%) (molar ratio Sr/P =1.67. By adding NH_4OH (Merck, 30%), the pH of the solution was adjusted to 9.0. A white precipitate was formed, and the suspension was stirred for 2 h. Thereafter, the precipitate was washed with distilled water and vacuum filtered **[22,23]**. The preparation reaction occurs according to the **equation (1)**.

$$10\ Sr\ (NO_3)_{2(aq)} + 6\ H_3PO_{4(aq)} + 2\ NH_4OH_{(aq)} \rightarrow Sr_{10}(PO)_6(OH)_{2(s)} + 18\ HNO_{3(aq)} + 2NH_4NO_{3(aq)} \text{-------(1)}$$

2.2. Preparation of BiOCl/SrHA

BiOl/SrHA nanoparticles were synthesized by a modified hydrothermal method using bismuth oxide, Hl, and SrHA as precursors. The Bi_2O_3 (1.5g) was dissolved in excess concentrated hydrochloric acid (10 mol/L, 10 mL) to obtain a transparent BiO_3-Hl aqueous solution. To this solution, 1.2 g of SrHA was added with simultaneous stirring. The obtained mixture was sonicated for 15 min. The pH of the solution was adjusted between 2 and 3 using ammonia. The mixture was heated at 90 ^oC for half an hour to obtain white precipitates. The precipitates were washed several times with water and ethanol and then dried at 75 ^oC for 10 h. The acquired product is calcined in an electric furnace for 3 h at 550 ^oC. to obtain BiOl/SrHA nanoparticles

3. Photocatalytic dyes degradation and reactor

A photoreactor (as seen in **Figure 2**) experiment was carried out in a mode photoreactor. It was irradiated with UV light using (λ=254nm, 30V). The photocatalytic dye's degeneration tests

were performed by mixing different number of BiOl/SrHA nanoparticles in a photoreactor with a capacity of 1000 mL of each dye solution (15, and 20 mg/L, respectively) at 25°c. At predictable time intervals, the solution patterns were removed from the reaction medium. With the use of a UV–vis spectrophotometer (Perkin-Elmer Lambda 25), we separate BiOl/SrHA from the solution and observe the change in the catalyst adsorption process for these dyes at maximum wavelengths 545 and 591 nm for Basic Fuchsin and Crystal Violet, correspondingly. The concentration of BiOl/SrHA nanoparticles has an effect on the degeneration of photocatalytic dyes by contacting 1000 mL of dye solution (15 and 20 mg/L for Basic Fuchsin and Crystal Violet, respectively) at room temperature of 25°C for 5 h. various number of BiOl/SrHA nanoparticles were used. The initial dye concentration was calculated to see how it affects photocatalytic dye degradation. The BiOl/SrHA nanoparticles (0.05 g Basic Fuchsin, and 0.05 g for Crystal Violet) were added to 1000 mL of different dye concentrations (15, 30, 45, and 60 mg/l) of Basic Fuchsin (BF) and (20, 40, 60, and 80 mg/l) of Crystal Violet (CV).

4. Result and discussion

4.1. Characterization of specimens

Figure 3 shows the FT-IR spectra of BiOl/SrHA, the range of (3417.98 – 3346.76) cm−1 may refer to the stretching vibrations of −OH that existed in the adsorbed water molecule. As well the distinctive peaks at range (1615.41) cm-1 are referring to the O-H bending vibrations. for pure BiOl, 442.73 cm−1 corresponds to valence symmetrical (A2u-type) vibrations of the Bi-O bond, a reference that the compounds of BiOl are obtained. The broadband at 3417.98 cm-1 is refer to O–H vibration of H_2O absorbed in the specimen. 1404.71 cm-1 peak is refer to the carbon-related pollution and a small amount of $(CO3)^{2-}$ caused by the CO2 in an aqueous solution or air during the synthesis. 1615.41 cm-1 peak is refer to carbon-related pollution. The bands at 1018.19 are a marker of asymmetric stretching. The two groups of bands in the low wavenumber ranging from 605.22-510.04 cm-1 are attributed to the bending vibrations of O–P–O in (PO4)3- groups. Confirmed the formation of BiOl/SrHA. **Figure 4** note sample BiOl/SrHA overlapped with each other. The morphology of BiOl/SrHAp diagnosed by scanning electron microscopy (SEM) are fixed in SEM visual data shows a quite different morphology. notable, the surface structure of BiOl/SrHA changes to marked rise with some holes which look like bunches of grapes that were not present before being installed when modified, this explains the presence of a large surface area, which increased the adsorption process of the dyes Basic Fuchsin, and Crystal Violet, widely used dyes, were chosen as the

test pollutant to evaluate the photocatalytic activity of synthesized BiOl/SrHA. The phase structures of the as-synthesis BiOl/SrHA specimens were examined by XRD. As displayed in **Figure 5** peaks from BiOI/SrHA sample appear at 13.1, 23, 27.3, 31.7, 32.8, 35.25, 39.95, 40.95, 42.95, 46.25, 49.55, and 58.53, 2θ values with corresponding hkl values as 002, 012, 110, 013, 004, 020, 005, 114, 122, 016, 025, and 017, respectively, as per JCPDS card No. 73-2062.**[20]**. describe the EDX pattern of BiOl and BiOl/SrHA. in **Figure 6**, The presence of the components O, P, I, Sr, and Bi in BiOl/SrHA verified its formation.

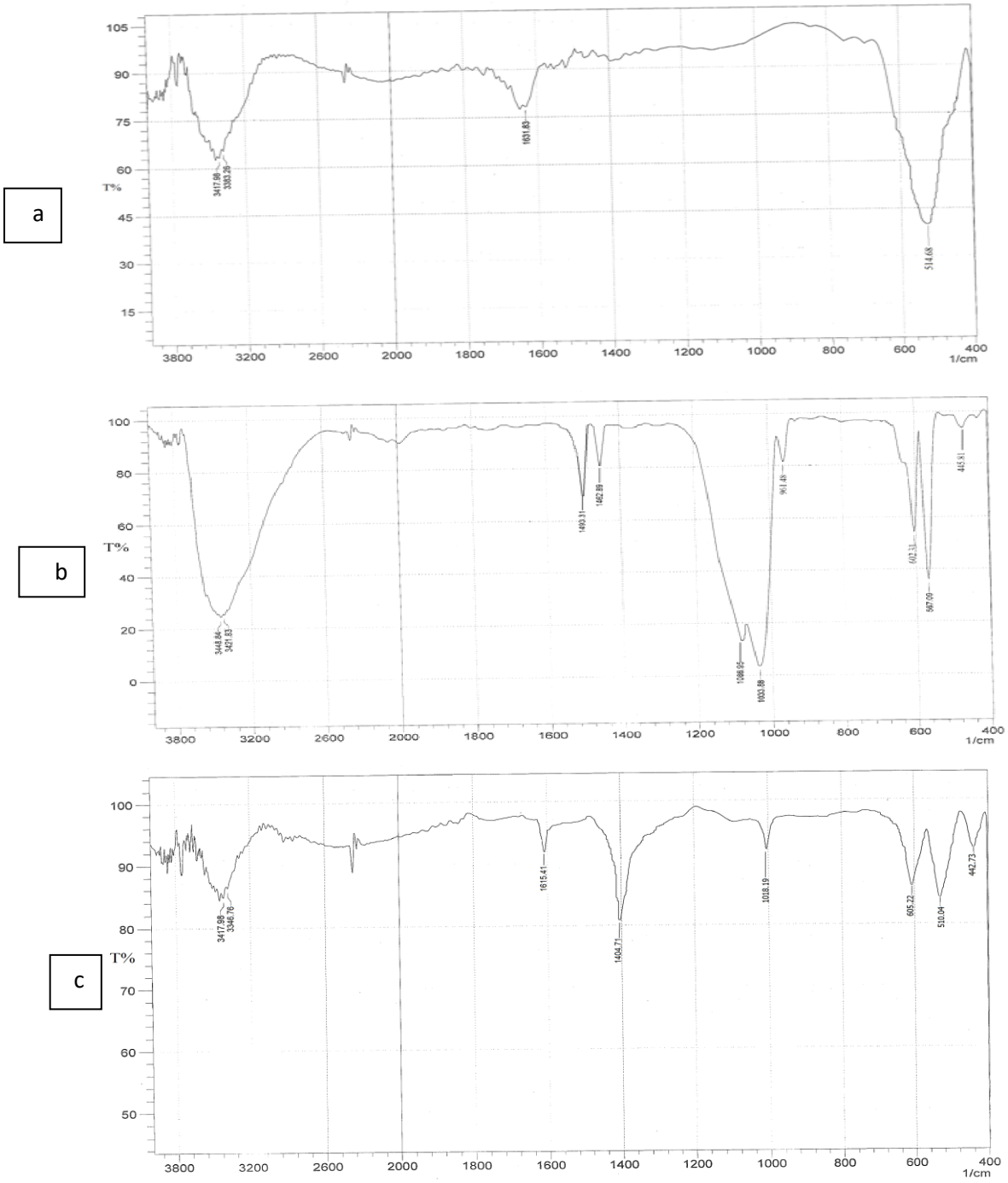

Figure 2: FTIR patterns of (a) BiOl, (b) SrHA, and (c) BiOl/SrHA

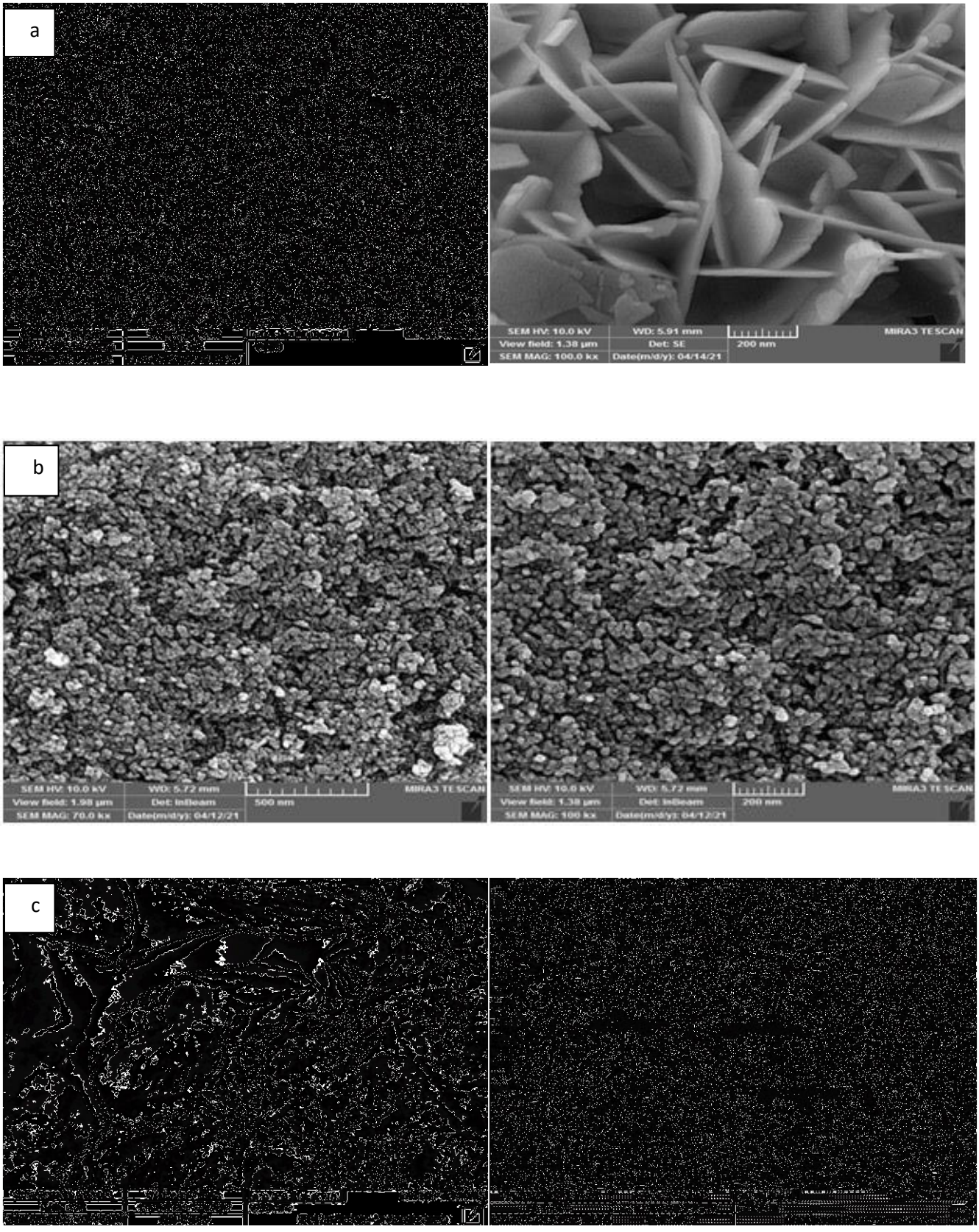

Figure 3: SEM of BiOl (a), SrHA (b) and BiOl/SrHA (c)

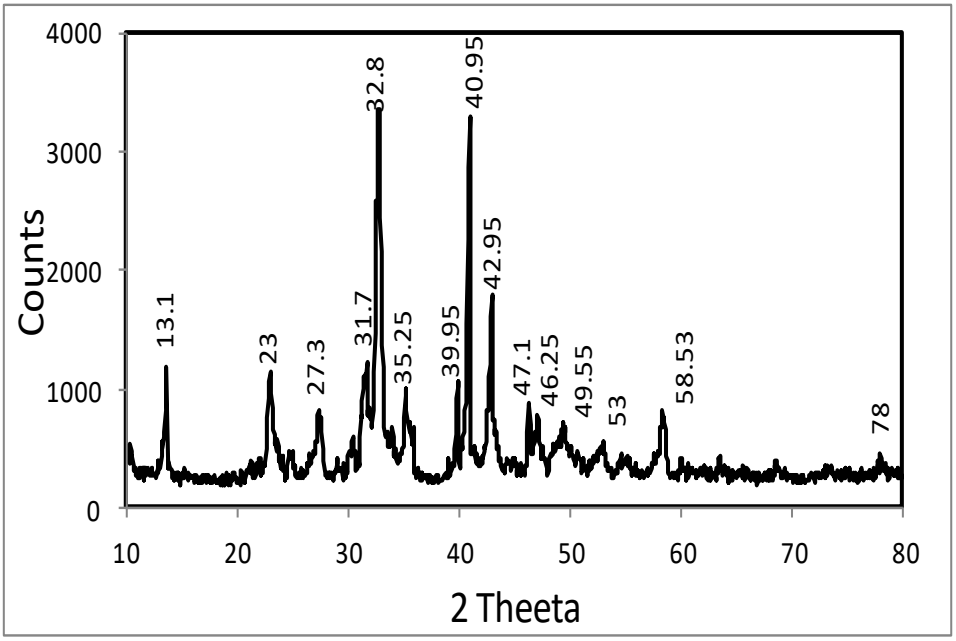

Figure 4: XRD patterns of BiOl/SrHA

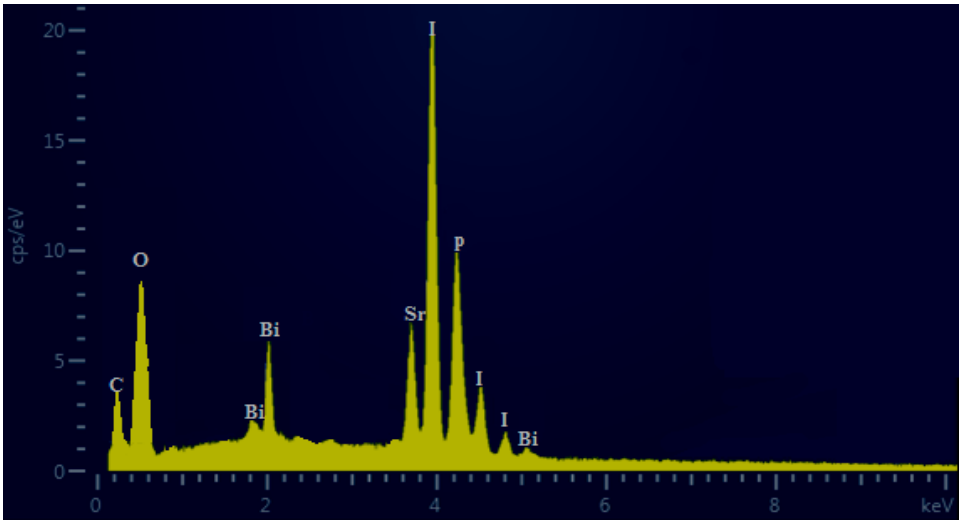

Figure 5: EDX pattern of BiOI/SrHA

5. Impact of some parameters on dyes degradation

5.1. Effect of BiOl/SrHA concentration

Figure 7 shows the effect of BiOl/SrHA concentration on photocatalytic dyes decomposition. In the absence of BiOl/SrHA, photodegradation for BF and CV is (5 and 3.5) %, correspondingly. Believing ultraviolet light alone was insufficient to oxidize dyes included in colourful wastewater samples; photocatalysts must be used to activate the UV. It is when the

use of BiOl/SrHA is as a photocatalyst with UV produces a significant improvement of dyes decay on the reverse when using UV alone to decomposition dyes [24]. The nanoparticles BiOl on SrHA as support are an experimentally efficient photocatalyst that uses light energy to form the e-/h+ pair on its surface. Where this pair e^-/h^+ leads to on decomposing the dyes through the formation of active oxygen superoxide radical anions ($O2^{\bullet-}$) and hydroxyl radicals ($HO^{\bullet}$) Which is the main sources in the pollutant decay. The kinetics of photocatalytic dye degradation by the photocatalyst BiOI/ SrHA were investigated at zero-order (eq. 2), first order (eq. 3), and second order (eq. 4).

$$Co - Ct = kot \quad \text{----------(2)}$$

Where Co and Ct are the initial and equilibrium concentration at any time dye concentration (mg/l), KO is the rate constant of pseudo-first order kinetic equation. The value of ko was determined from the slope of the linear plots of Co-Ct vs t.

$$\frac{dq}{dt} = k1(q_e - q_t) \quad \text{----------(3)}$$

The integrated form of the above expression is (4):

$$Ln(q_e-q_t) = lnq_e - k_1t \quad \text{----------(4)}$$

Where k_1 (min^{-1}) is the rate constant of pseudo-first order kinetic equation, qe and qt, respectively are the amounts of adsorbate adsorbed at equilibrium and at any time (mg /g). The value of k_1 was determined from the slope of the linear plots of ln ($q_e - q_t$) vs t.

$$\frac{t}{qt} = 1/k_2q_e + t/q_e \quad \text{----------(5)}$$

Where k_2 (g mg^{-1} min^{-1}) is the rate constant of pseudo-second order kinetic equation. The value of qe and k_2 can be determined by the slopes and intercepts of the straight line of the plots (t/q_t vs t).

The insertion of the applicability of pseudo zero, first, and second-order kinetics models for photocatalytic dye degradation by the nanoparticles of BiOX (X= Cl, Br, or I)/SrHA at different catalyst dosages, ko, k1, and k2 and R2 (correlation coefficient values) are shown in Table 1 respectively. The results shown in that the kinetics of photo catalytic dye degeneration via BiOX (X= Cl, Br, or I)/SrHA at various catalyst dosages followed the first-order kinetics.

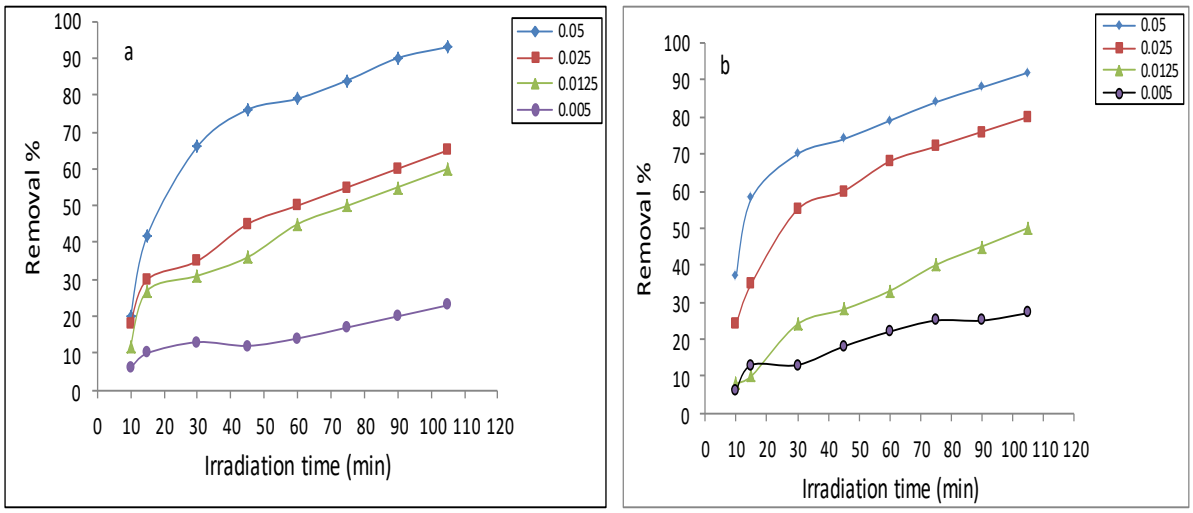

Figure 6: The effect of BiOl/SrHA concentration on the degradation of dyes in the presence of UV/BiOl/SrHA BF(a) and CV(b)

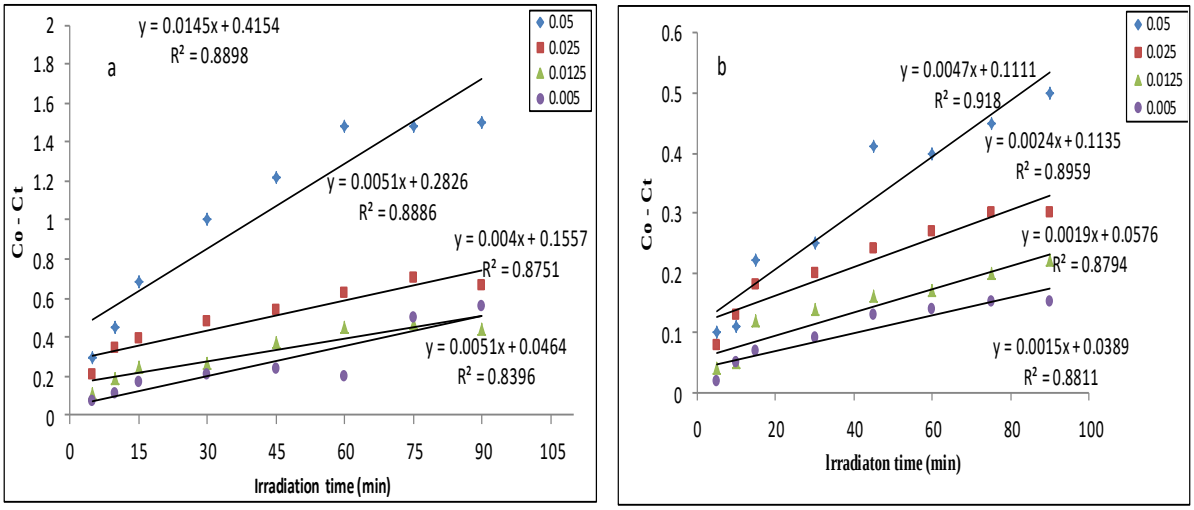

Figure 7: Shows the zero-order kinetics of photocatalytic dye degradation using BiOl/SrHA at varied catalyst concentrations BF(a) and CV (b)

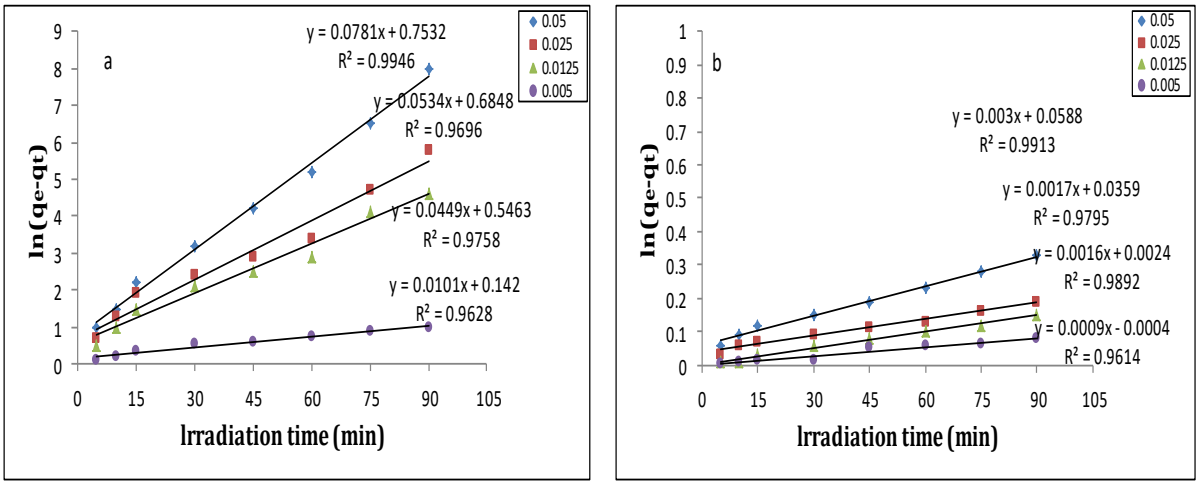

Figure 8: Shows the first-order kinetics of photocatalytic dye degradation using BiOl/SrHA at varied catalyst concentrations BF(a) and CV (b)

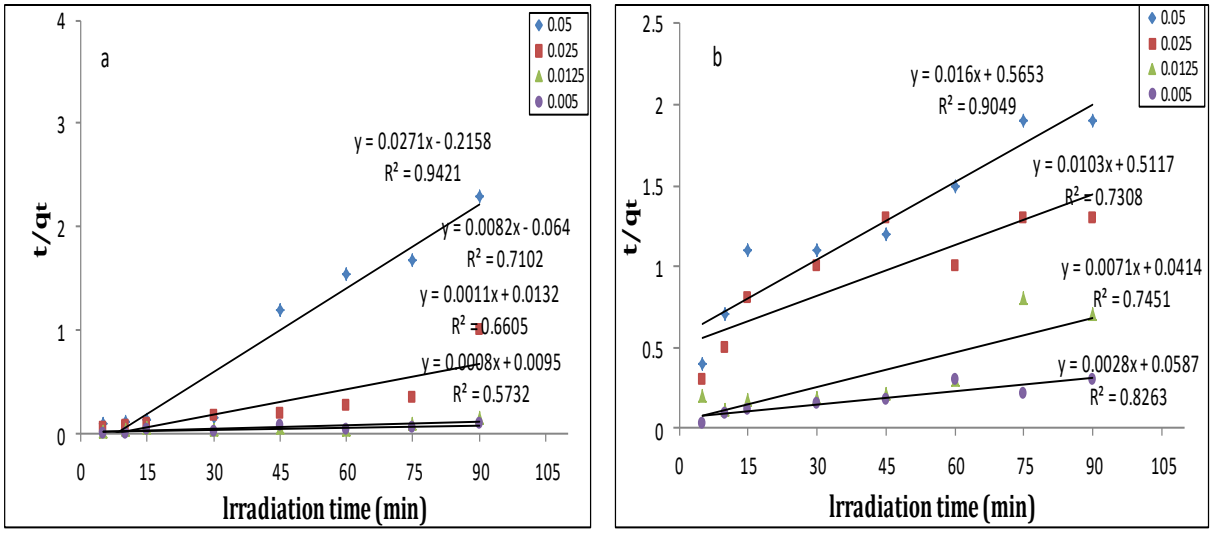

Figure 9: Shows the second-order kinetics of photocatalytic dye degradation using BiOl/SrHA at varied catalyst concentrations BF(a) and CV (b)

Table 1: The kinetics constants of photocatalytic Basic Fuchsin dye degradation by BiOl/SrHA at various catalyst dosages

BiOI/SrHA(g)	Pseudo-zero order		Pseudo-first order		Pseudo-second order	
BF	K_0	R^2	K_1	R^2	K_2	R^2
0.05	0.0145	0.8898	0.0781	0.9946	0.0034	0.9421
0.025	0.0051	0.8886	0.0543	0.9696	0.0010	0.7102
0.0125	0.004	0.8751	0.0449	0.9758	9.1E-05	0.6605
0.005	0.0051	0.8396	0.0101	0.9628	6.7E-05	0.5732
VC						
0.05	0.0047	0.918	0.003	0.9913	0.0004	0.9094
0.025	0.0024	0.8959	0.0017	0.9795	0.0002	0.7308
0.0125	0.0019	0.8794	0.0016	0.9892	0.0012	0.7451
0.005	0.0015	0.8811	0.0009	0.9614	0.0001	0.8263

5.2. Initial dye concentration

Figure 11 shows the effect of initial dye concentration on the photocatalytic dye decomposition at various time intervals. The results show that dye degradation decreases through initial dye concentration increasing. With the increase in the dye concentration, the potential reason is the intervention from intermediates composed upon the decay of the parental dye molecules. The degradation inhibition repression would be more obvious in the presence of a high level of degradation intermediates composed of an increased initial dye concentration **[25]**. Used equations of the zero-order, first order, and second-order kinetics types for photocatalytic dye degradation by the nanoparticles at various initial dye concentrations, linear plots of C_o - C versus irradiation time (t) for zero-order model **Figure 11**, ln (C_o/C) versus irradiation time (t) for first-order order model **Figure 12**, and 1/C against irradiation time (t) for second order type of **Figure 13** are plotted. The values of ko, k_1, and k_2, R^2 (correlation coefficient values) are shown in **Tables 2**. The outcome showed that the kinetics of photocatalytic dye degeneration by BiOl/SrHA at various initial dye concentrations followed the first-order kinetic type.

The following experiments were performed at pH 7 and temperature 30±5 ^oC.

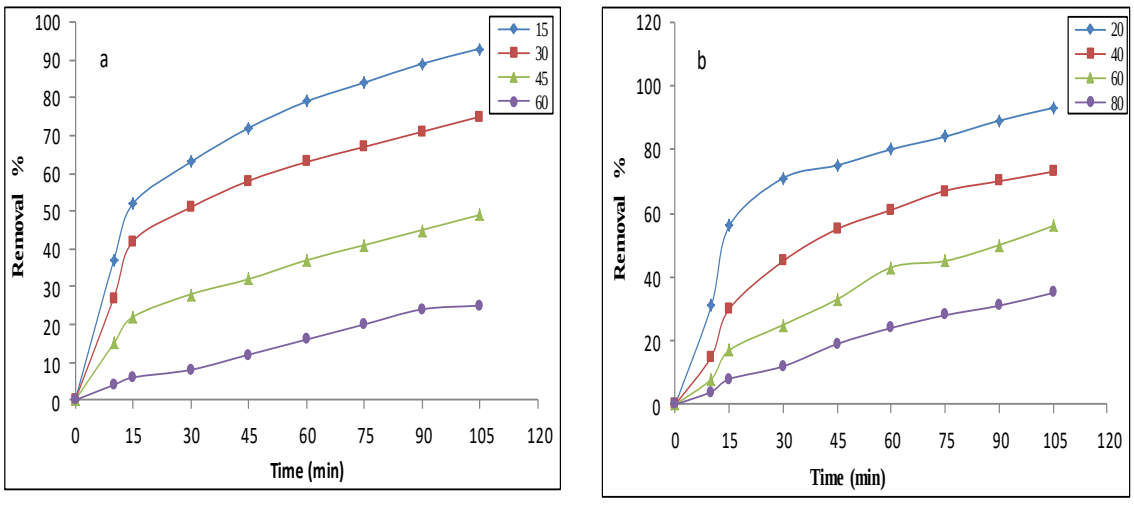

Figure 10: dye concentration effect on the degradation of dyes using UV/BiOI/ SrHA (a) BF, and (b) CV

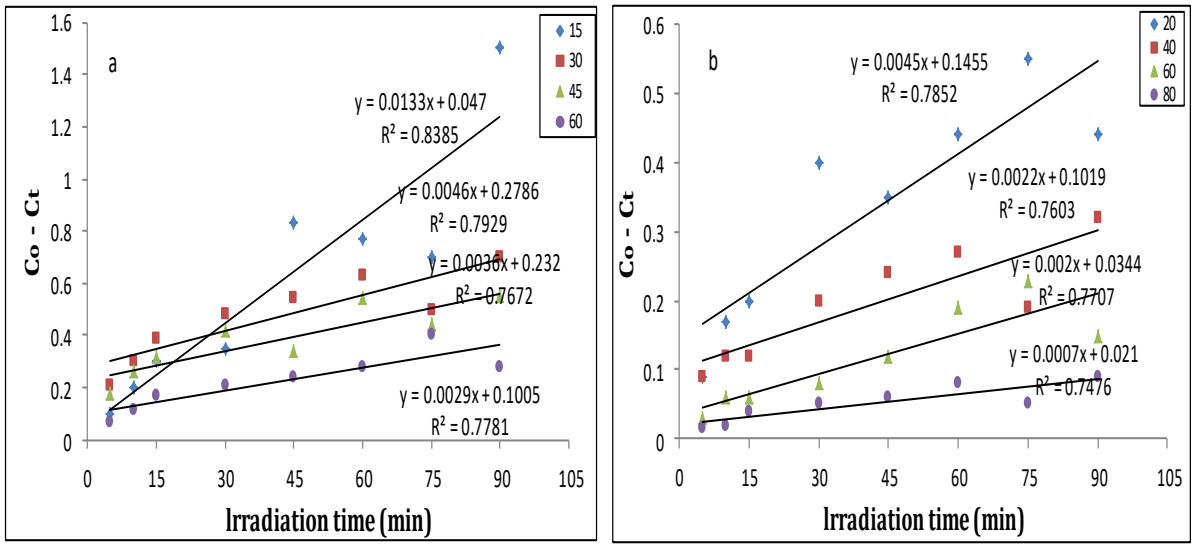

Figure 11: The zero-order kinetic of photocatalytic dye degradation by BiOI/ SrHA different dye concentrations (a) BF, and (b) CV

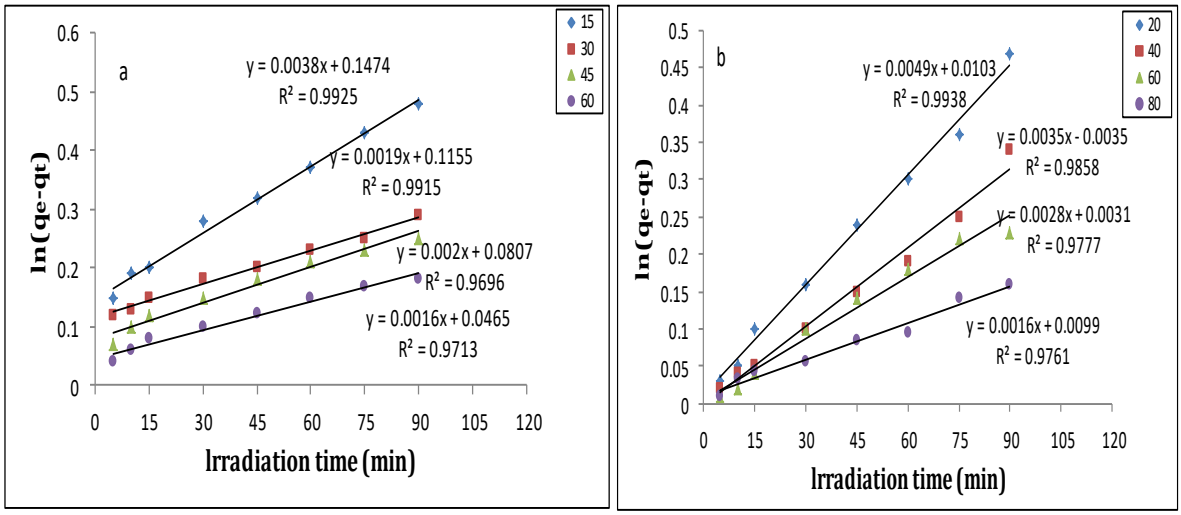

Figure 12: The first-order kinetic of photocatalytic dye degradation by BiOI/ SrHA different dye concentrations (a) BF, and (b) CV

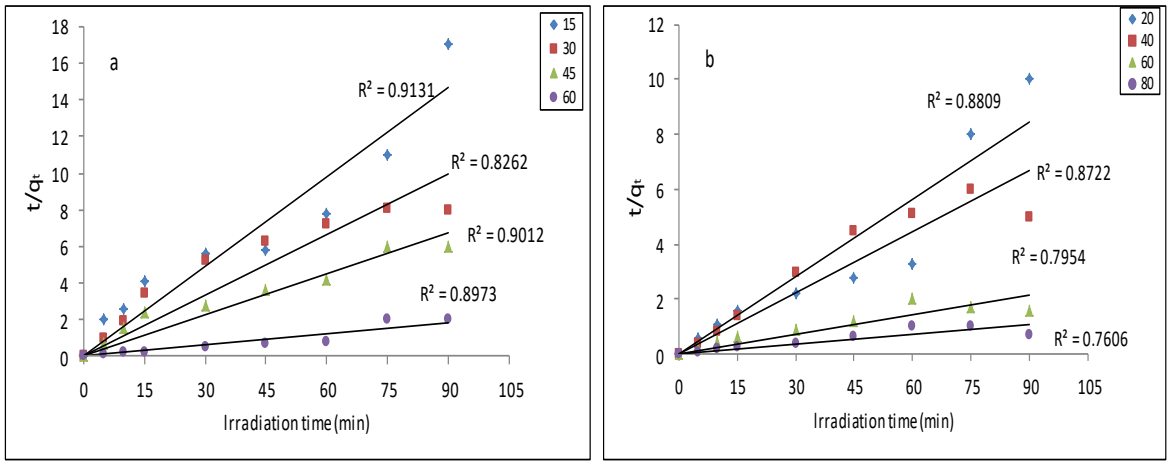

Figure 13: The second-order kinetic of photocatalytic dye degradation by BiOI/ SrHA different dye concentrations (a) BF, and (b) CV

Table 2: The kinetics constants of photocatalytic dye degradation by BiOl/SrHA at various Basic Fuchsin and Crystal Violet dye concentrations

dye (mg/l)	Pseudo-zero order		Pseudo-first order		Pseudo-second order	
BF	K_0	R^2	K_1	R^2	K_2	R^2
15	0.0133	0.8385	0.037	0.9925	0.0002	0.9189
30	0.0046	0.7929	0.0295	0.9865	9.2E-05	0.8456
45	0.0036	0.7672	0.0191	0.9468	0.00016	0.8178
60	0.0029	0.7781	0.0112	0.9852	0.00017	0.7685
CV						
20	0.0045	0.7852	0.0528	0.9809	0.0011	0.9200
40	0.0022	0.7603	0.0361	0.9715	0.0013	0.9028
60	0.002	0.7707	0.0197	0.9776	0.0014	0.8636
80	0.0007	0.7476	0.008	0.9614	0.0023	0.7801

6. Conclusion

The results show that BiOI-supported SrHA is an efficient adsorbent for the removal of Basic Fuchsin (BF) and Crystal Violet (CV) dyes from aqueous solutions, and because of its higher capacity, it can be used in wastewater treatment. The increased photocatalytic activities of BiOI/SrHA could be referred to as the formation of a heterojunction between BiOI and SrHA, which helpfully restrains the recombination of electron-hole pairs. Both the photocatalytic process and the photosensitizer process would work concurrently, $^{\bullet}OH$ and $O_2^{-\bullet}$ are the two main active types in the photocatalytic process. In the photocatalytic process, N-de-methylation and conjugated structure of CV and BF dyes occur during the decomposition process with BiOI/SrHA starting the catalyst. Therefore, it can be concluded that BiOI/SrHA provides a heterogeneous surface for the adsorption of dyes. The outcome displays that the modified adsorbent is a strong UV photocatalyst.

7. REFERENCES

[1] Rakness, Kerwin L., et al. "Wastewater disinfection with ozone-process control and operating results." Ozone: science & engineering 15.6 (1993): 497-513.

[2] Raizada, Pankaj, et al. "Fabrication of Ag3VO4 decorated phosphorus and sulphur co-doped graphitic carbon nitride as a high-dispersed photocatalyst for phenol mineralization and E. coli disinfection." Separation and purification technology 212 (2019): 887-900.

[3] Pare, Brijesh, Pardeep Singh, and S. B. Jonnalagadda. "Visible light-driven photocatalytic degradation and mineralization of neutral red dye in a slurry photoreacter." (2010).

[4] B. Pare, P. Singh, S.B Jonnalagadda, Artificial light assisted photocatalytic degradation oflissamine fast yellow dye in ZnO suspension in a slurry batch reactor, Indian J. Chem., Sect A 48 A (2009) 1364-1369

[5] Zhang, Lisha, et al. "Sonochemical synthesis of nanocrystallite Bi2O3 as a visible-light-driven photocatalyst." Applied Catalysis A: General 308 (2006): 105-110.

[6] Asahi, R. Y. O. J. I., et al. "Visible-light photocatalysis in nitrogen-doped titanium oxides." science 293.5528 (2001): 269-271.

[7] Khan, Shahed UM, Mofareh Al-Shahry, and William B. Ingler. "Efficient photochemical water splitting by a chemically modified n-TiO2." science 297.5590 (2002): 2243-2245.

[8] Al-Rubaie, Ali Z., Inas K. Mohammed, and Zaki N. Kadhim. "Synthesis and Characterization of New Organotellurium (IV) Compounds Containing Carbodithioate Ligands." IOP Conference Series: Materials Science and Engineering. Vol. 928. No. 5. IOP Publishing, 2020.

[9] Singh, Pardeep, et al. "Preparation of BSA-ZnWO4 nanocomposites with enhanced adsorptional photocatalytic activity for methylene blue degradation." International Journal of Photoenergy 2013 (2013).

[10] Li, Shijie, et al. "A novel heterostructure of BiOI nanosheets anchored onto MWCNTs with excellent visible-light photocatalytic activity." Nanomaterials 7.1 (2017): 22.

[11] Xiang, Yuhui, et al. "Chemical etching preparation of the Bi2WO6/BiOI p–n heterojunction with enhanced photocatalytic antifouling activity under visible light irradiation." Chemical Engineering Journal 288 (2016): 264-275.

[12] Chen, Lang, et al. "Room-Temperature Synthesis of Flower-Like BiOX (X⍰ Cl, Br, I) Hierarchical Structures and Their Visible-Light Photocatalytic Activity." Inorganic chemistry 52.19 (2013): 11118-11125.

[13] Radhi, Ibtighaa Kadhim, Mouayed Abdulaali Hussein, and Zaki Naser Kadhim. "Investigation of nigrosine, alizarin, indigo and acid fuchsin removal by modification of CaO derived from eggshell with AgI: Adsorption, kinetic and photocatalytic studies." *European Journal of Chemistry* 10.1 (2019): 64-71.

[14] Jiang, Zaiyong, et al. "Enhancing visible light photocatalytic degradation performance and bactericidal activity of BiOI via ultrathin-layer structure." Applied Catalysis B: Environmental 211 (2017): 252-257.

[15] Luan, Jingfei, et al. "Growth, structural and photophysical properties of i2GaTaO7."

Journal of crystal growth 273.1-2 (2004): 241-247.

[16] Di, Jun, et al. "Bidirectional acceleration of carrier separation spatially via N-CQDs/atomically-thin BiOI nanosheets nanojunctions for manipulating active species in a photocatalytic process." Journal of Materials Chemistry A 4.14 (2016): 5051-5061.

[17] Jiang, Zaiyong, et al. "Enhancing visible light photocatalytic degradation performance and bactericidal activity of BiOI via ultrathin-layer structure." Applied Catalysis B: Environmental 211 (2017): 252-257.

[18] Di, Jun, et al. "Reactable ionic liquid-assisted rapid synthesis of BiOI hollow microspheres at room temperature with enhanced photocatalytic activity." Journal of Materials Chemistry A 2.38 (2014): 15864-15874.

[19] Hasan, Jaafar, et al. "Efficient visible-light-driven photocatalysis of flower-like composites of AgI nanoparticle dotting BiOI nanosheet." Journal of Solid-State Chemistry 297 (2021): 122044.

[20] Ye, Liqun, et al. "Synthesis of highly symmetrical BiOI single-crystal nanosheets and their {001} facet-dependent photoactivity." Journal of Materials Chemistry 21.33 (2011): 12479-12484.

[21] Xiao, Xiufeng, et al. "Structural characterization of zinc-substituted hydroxyapatite prepared by hydrothermal method." Journal of materials science: Materials in medicine 19.2 (2008): 797-803.

[22] Radhi, Ibtighaa Kadhim, Mouayed Abdulaali Hussein, and Zaki Naser Kadhim. "Investigation of nigrosine, alizarin, indigo and acid fuchsin removal by modification of CaO derived from eggshell with AgI: Adsorption, kinetic and photocatalytic studies." European Journal of Chemistry 10.1 (2019): 64-71.

[23] AS Alassadi, Erfan, Zaki N Kadhim, and Mazin N Mousa. "The In Vitro Release Study Of Ceftazidime drug From Synthesized Strontium Flourapatite And Strontium Hydroxyapatite Coated Particles." *karbala journal of pharmaceutical sciences* 8.13 (2017): 137-151.

[24] Simon, V., et al. "Microscopic analysis of sintered titanium-hydroxyapatite implant materials." Journal of Optoelectronics and Advanced Materials 7.6 (2005): 2823.

[25] Kumar, Ankit, and G. Pandey. "A review on the factors affecting the photocatalytic degradation of hazardous materials." Mater. Sci. Eng. Int. J 1.3 (2017): 1-10.